

Impact of residual doping on surface current of InGaAs/InP photodiode passivated with regrown InP

Oswaldo M. Braga^{1*}, Cristian A. Delfino¹, Rudy M. S. Kawabata², Luciana D. Pinto², Gustavo S. Vieira¹, Mauricio P. Pires³, Patricia L. Souza², Euclides Marega⁴, John A. Carlin⁵, Sanjay Krishna⁵

¹Institute for Advanced Studies, IEAV, 12228-001, São Paulo, Brazil

²LabSem, CETUC, Pontifícia Universidade Católica, PUC-Rio, R. Marquês de São Vicente 124, Gávea, 22451-900 Rio de Janeiro, Brazil

³Physics Institute, Federal University of Rio de Janeiro, Av. Athos da Silveira Ramos 149, 21941-909 Rio de Janeiro, Brazil

⁴Universidade de São Paulo, USP-São Carlos, 13566-560 São Carlos, SP, Brazil

⁵Ohio State University, 281 W Lane Ave., Columbus, OH 43210, USA

Article info

Article history:

Received 15 Oct. 2022

Received in revised form 22 Dec. 2022

Accepted 17 Jan. 2023

Available on-line 24 Feb. 2023

Keywords:

Simulation; residual doping; recombination velocity; surface passivation; regrowth.

Abstract

The viability of epitaxial regrowth of non-intentionally doped InP to passivate lateral mesa surfaces of InGaAs photodiodes lattice-matched to InP is investigated, evaluating whether the residual doping of the regrown layer can be responsible for an unexpected increase of the surface current. The effect of residual doping is evaluated via numerical calculations of dark current, considering the range of doping concentrations expected for non-intentionally doped InP. The calculations show that the increase in dark current due to the residual doping of the regrown InP layer is not enough to justify the observed increase in surface current. On the other hand, the technique is still valid as a passivation method if the photodetector pixel is isolated by etching only the top contact layer.

1. Introduction

InGaAs photodiodes lattice-matched to InP are good photodetectors for applications such as defence, medicine, fibre optic communication, and industry [1–3] and they have been extensively studied for the short-wavelength infrared (SWIR) [4–8]. The layers of this type of structure are produced through a high-quality epitaxial growth process that results in low dark current densities and large quantum efficiency in this wavelength range [9].

Lattice-matched InGaAs photodiodes are mainly done by diffusion of p-type dopant through a higher gap semiconductor. It is done to reduce dark current and improve its stability. The reason why the dark current is smaller is that the junction surface is in a semiconductor of a wider bandgap in this configuration. In principle, a similar way of doing so is to fabricate a mesa-type photodiode and regrow a lattice-matched wider gap semiconductor on the mesa sidewalls. To such a strategy

work, the regrown layer and its interface with the previous device layers must be of high quality. Since the surface states usually act as non-radiative relaxation centres for electron-hole recombination, photoluminescence (PL) can be used as a reference to this density of states.

The best-performing InGaAs photodiodes have been fabricated in a planar geometry, however, mesa-defined devices are interesting and enable more complex structures such as multiwavelength stacked photodetectors. Nonetheless, while many techniques have been tried for passivating lateral mesas of lattice-matched InGaAs photodiodes, to date, none have succeeded in making the surface leakage negligible when a very low bulk leakage is achieved [10–12]. These attempts include sulphur and dielectric passivation. These processes remove the native oxides and passivate the dangling bonds on the exposed InGaAs surface.

In previous work, the authors have shown that epitaxially regrown InP reduced the surface recombination velocity (SRV) strongly, but it did not reduce the reverse dark current of deep mesa devices [13]. It was suggested

*Corresponding author at: ombrega@gmail.com

that the residual doping of the regrown layer was the most plausible cause for the apparent contradiction. Here, this hypothesis is evaluated by calculating the dark current as a function of residual doping of the regrown layer.

2. Experiment

The p-i-n photodiodes of $\text{In}_{0.53}\text{Ga}_{0.47}\text{As}$, lattice-matched to InP, were grown by a metalorganic vapour-phase epitaxy (MOVPE). The structure consists of a 200 nm $\text{In}_{0.53}\text{Ga}_{0.47}\text{As}$ top contact layer (Zn doped with a density of $2 \cdot 10^{18} \text{ cm}^{-3}$), a 2.0 μm non-intentionally doped (NID) $\text{In}_{0.53}\text{Ga}_{0.47}\text{As}$ absorption layer and a 200 nm base contact InP layer (Si doped with a density of $2 \cdot 10^{18} \text{ cm}^{-3}$), over a semi-insulating (Fe-doped) InP substrate.

The authors have produced two mesa designs using a two-step ICP-RIE dry etch: in the first step, the top InGaAs contact layer was etched (shallow mesa) and in the second step, the structure was etched down closer (leaving about 400 nm of InGaAs to allow selective etching of the regrown InP, since the bottom contact layer is also InP) to the base contact (deep mesa), with different patterns for the two designs, producing two different groups of mesas (Figs. 1 and 2). After etching, the samples were cleaned and a 200 nm thick NID InP layer was regrown uniformly on the processed wafer, by MOVPE. This was further selectively etched dividing each group into two subgroups of passivated and un-passivated devices, each one with 11 square mesas with side sizes in the range from 15 μm to 500 μm for shallow mesas and from 25 μm to 510 μm for deep mesas (the second etch adds 10 μm to mesas side length). Additionally, the sample was covered with SiO_2 , and deposited by plasma-enhanced chemical vapour deposition (PECVD), for insulation purposes, and it was selectively etched, leaving SiO_2 on the top of the regrown layer. The contact pads were placed next to the mesas, over the SiO_2 , and metal trails connected them to the top contact (InP and SiO_2 were not totally removed but kept as an

insulator under the metal pads and trails to the top of un-passivated devices). The structure and fabrication process are presented in more detail in the previous work [13].

The deep mesas, with different sizes, were produced to distinguish the two components of the dark current of the devices (the bulk and the surface current on the sidewalls of the device). The active area for a photocurrent collection of the shallow etched devices is defined by the geometric area plus one diffusion length of minority carriers (holes) surrounding it [14], but the current density is given by the geometric area, although the surrounding area contributes to both, dark current and photocurrent. Using the optical area as an area for the dark current of shallow devices is a way of computing the leak current beyond thermally generated minority charges in the surrounding area. To evaluate the passivation technique through the comparison of the passivated and un-passivated regions of the absorber layer, the shallow mesas were fabricated. This evaluation consisted of PL measurement and lateral photocurrent collection.

In Fig. 3, the top view of a group of mesas can be observed. The darker grey region is the passivated area where the sidewalls of the photodiodes are covered with regrown InP and SiO_2 .

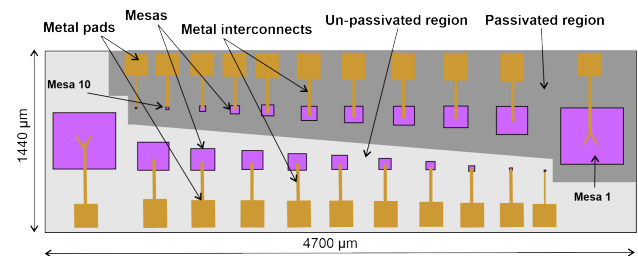


Fig. 3. Groups of passivated and un-passivated mesas with different sizes. Similar groups for shallow and deep mesas were fabricated.

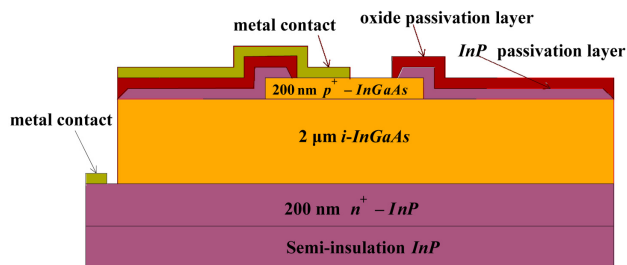


Fig. 1. Side view of a shallow mesa showing the passivation layers.

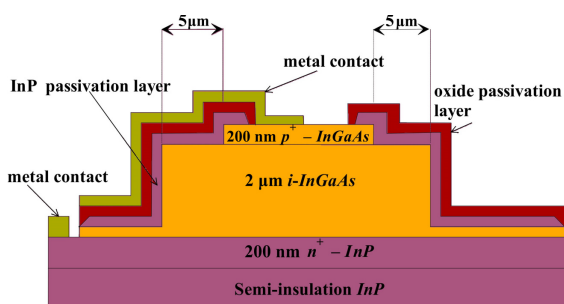


Fig. 2. Side view of a deep mesa showing the passivation layers.

3. PL and dark current measurements

The PL measurements published before indicated that the passivation with regrown InP reduces non-radiative recombination [13]. The dark current on devices was measured to analyse the current on sidewalls of the different deep mesas. The data showed that the surface component of the dark current is dominant. The dark current increased on the deep mesa passivated devices, instead of decreasing, as can be seen in Figs. 4 and 5 for a group of deep mesas, at room temperature. Using the traditional plot of current density vs. perimeter/area ratio, it is possible to extract the value for the perimeter leakage current density (Fig. 4). The slope, corresponding to the perimeter leakage current density at deep mesas, is $0.20 \pm 0.03 \text{ A}\cdot\text{cm}^{-1}$ for un-passivated devices and $0.94 \pm 0.04 \text{ A}\cdot\text{cm}^{-1}$ for passivated devices. In Figs. 6 and 7, the dark current was measured on the shallow devices to try to understand the conflicting results. For extracting the slope for shallow mesas (Fig. 6), the authors have assumed that the mesa effective area is a single photodiode square mesa with lateral minority diffusion length surrounding de mesa. The values for lateral minority diffusion length for passivated and un-passivated devices were obtained via lateral photocurrent collection in a previous work [15]. The

values obtained for the perimeter leakage current density at shallow mesas are $4.4 \pm 0.3 \text{ A}\cdot\text{cm}^{-1}$ for un-passivated devices and $0.00 \pm 0.08 \text{ A}\cdot\text{cm}^{-1}$ for passivated devices (in this case, showing a very small value, smaller than the standard error). The results observed in the shallow mesas show a significant dark current reduction, implying that it is possible to use such a technique to produce focal plane arrays (FPAs) with the pixels isolated by etching only the top contact.

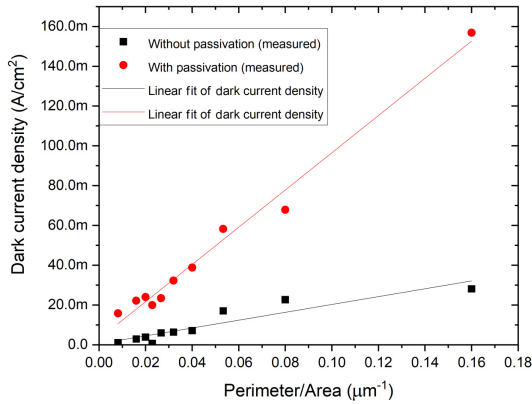


Fig. 4. Reverse dark current measured at -1 V and at room temperature vs. perimeter-to-area ratio for deep mesa with and without passivation.

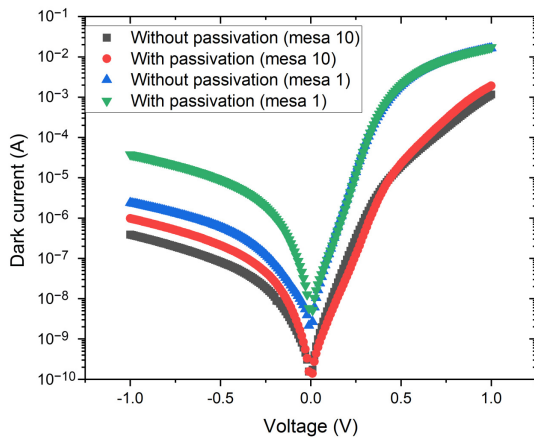


Fig. 5. The experimental dark current of the photodiode for deep mesa 1 ($510 \times 510 \mu\text{m}^2$) and deep mesa 10 ($35 \times 35 \mu\text{m}^2$), at room temperature.

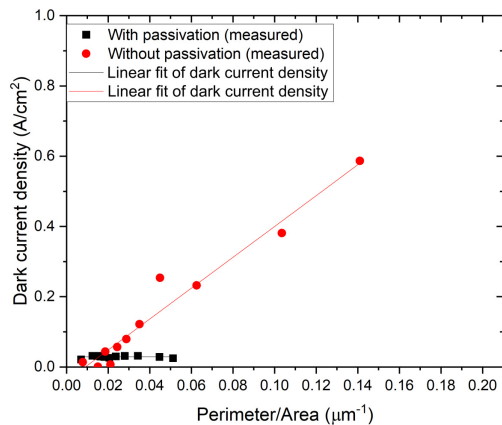


Fig. 6. Reverse dark current measured at -1 V and at room temperature vs. perimeter-to-area ratio for shallow mesa with and without passivation.

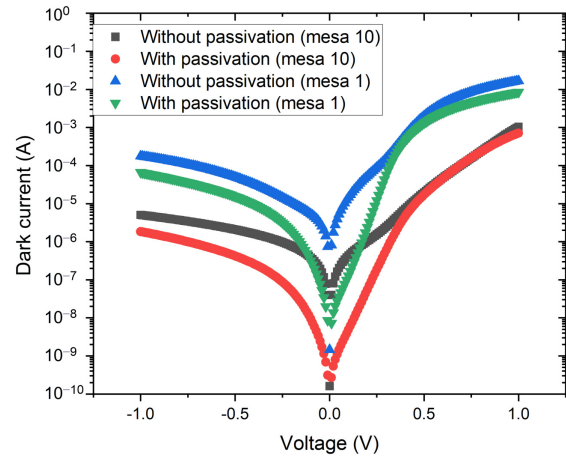


Fig. 7. The experimental dark current of the photodiode for shallow mesa 1 ($500 \times 500 \mu\text{m}^2$) and shallow mesa 10 ($25 \times 25 \mu\text{m}^2$), at room temperature.

Since the InP layer quality on the sidewalls of the mesas could eventually be different from the quality obtained on the top surface, the morphology of the layer at the side walls was verified by scanning electron microscopy showing a smooth surface, without visible defects [13], and this led the authors to suggest another hypothesis. Considering that the regrown InP layer is NID and that such layer usually has residual n-type doping of the order of 10^{15} to 10^{16} cm^{-3} [16, 17], this residual electron concentration will be transferred to the InGaAs layers due to the gap difference and could be the cause of the higher dark current in deep mesas (Figs. 4 and 5). The following calculations aim to verify if residual doping of the InP passivation layer in the expected range can generate the observed dark current increase in the deep mesa devices.

4. Current calculation

Dark current modelling was developed using two-dimensional device simulator Silvaco Atlas [18] and the simulation was conducted for the device shown in Fig. 8. The material parameters of InP, InGaAs, and SiO_2 are based on the values found in the literature (Table 1). The value of bulk lifetime used for the absorber layer and the SRV applied to the InGaAs/regrown InP interface were determined in a previous work [15]. The devices were simulated by using the drift-diffusion model, the dependence of carrier lifetime on doping density, the dependence of mobility on the low field, the Shockley–Read–Hall (SRH)

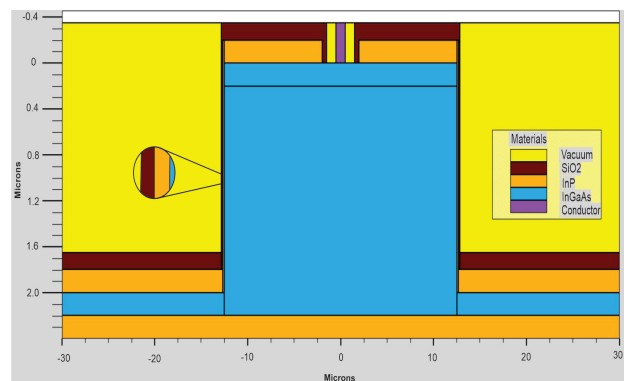


Fig. 8. Simulated 2D structure in Silvaco Atlas.

recombination model, and the deep trap-assisted tunnelling (TAT) model [18]. To achieve a better simulation, a typical interfacial trapped charges density on the regrown InP/SiO₂ interface was applied [19] and, initially, the simulation was validated with the experimental dark current (I - V characteristics) for the shallow mesas without passivation, considering the trap parameters (concentration, deep level, and capture cross sections) in the absorber layer for fitting. After that, the simulation was applied to the passivated deep mesa. Table 1 shows the parameters utilized in the simulation.

Table 1.
Silvaco simulation parameters.

Parameter	Unit	Value	Ref.
In _{0.53} Ga _{0.47} As bandgap	eV	0.75	20
Trap energy level	eV	$E_c - 0.16$	21
Trap concentration	cm ⁻³	$3.5 \cdot 10^{13}$	21
Electron capture cross-section	cm ⁻²	$4.0 \cdot 10^{-17}$	21
Hole capture cross-section	cm ⁻²	$1.8 \cdot 10^{-17}$	21
TAT effective mass		$0.041 m_0$	20
In _{0.53} Ga _{0.47} As NID hole lifetime	μs	1.4	15
InP/SiO ₂ interface charge density	cm ⁻²	$1 \cdot 10^{12}$	19
SRV (regrown InP/InGaAs NID)	cm ² ·s ⁻¹	$(3.7 \pm 0.1) \cdot 10^4$	15
In _{0.53} Ga _{0.47} As hole mobility	cm ² V ⁻¹ s ⁻¹	300	20

4.1. Electron concentration

The electron concentration at room temperature calculated in the middle of the sidewall at different doping concentrations at the interface between NID InGaAs and the regrown InP is shown in Fig. 9. Considering a NID InGaAs absorber layer doping concentrations as $2 \cdot 10^{15}$ cm⁻³, as expected the free charge at the InGaAs (NID)/regrown InP interface increases with a doping of the regrown layers, but it is necessary to verify if this free charge is enough to generate the observed increase in dark current. For doing so, the dark current of the device was calculated for various residual doping concentrations in the InP regrown layer.

4.2. Dark current simulation

The experimental and calculated dark current-voltage (I - V) curves of a photodiode from -1 V to 0.5 V with different InP regrown layer doping concentrations at room temperature are shown in Fig. 10. It can be observed that although doping concentrations of the regrown InP present an influence on the reverse dark current, considering the NID InP regrown layer doping concentrations in the whole expected range results in a calculated dark current far below the measured dark current, showing that the residual doping should not be accounted as the main cause of the higher dark current in the passivated deep mesas.

Figure 11 presents the dark current density in the device when subjected to a bias of -0.5 V.

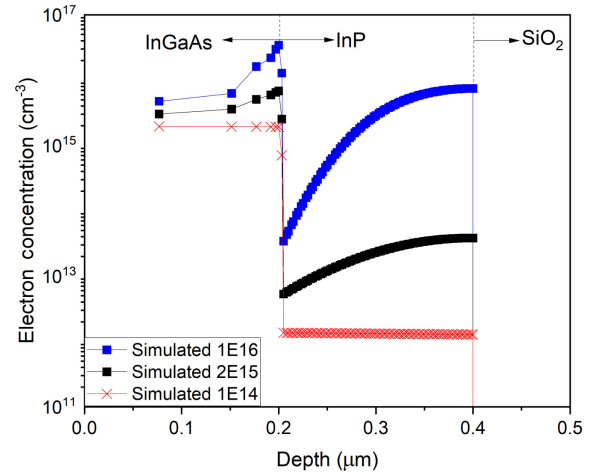


Fig. 9. Simulated electron concentration at the heterojunction, InGaAs NID/InP(regrown), on the sidewall (at half height) at a bias of 0 V, with a different InP regrown layer n-type doping concentrations (from $1.0 \cdot 10^{14}$ to $1.0 \cdot 10^{16}$ cm⁻³) and at room temperature.

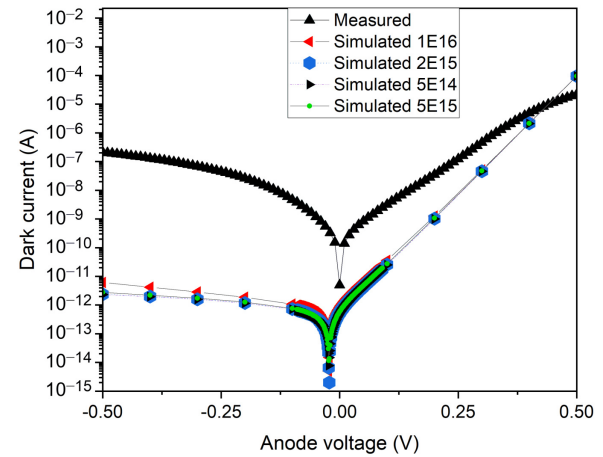


Fig. 10. The simulated and experimental dark current of the photodiode for deep mesa of 35×35 μm², at different InP regrown layer n-type doping concentrations (from $5.0 \cdot 10^{14}$ to $1.0 \cdot 10^{16}$ cm⁻³) at room temperature.

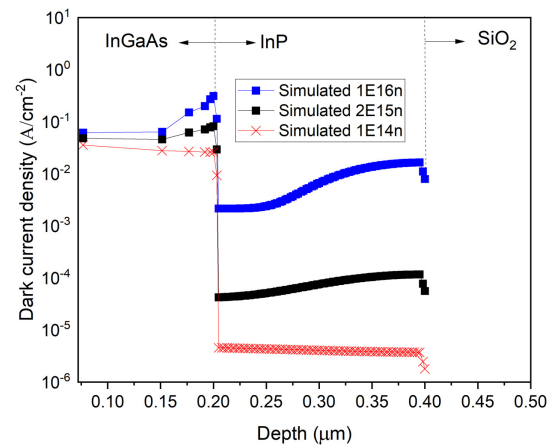


Fig. 11. The dark current density distribution of the heterojunction InGaAs NID/InP(regrown) on the sidewall (at half height) at a bias of -0.5 V, at different InP regrown layer n-type doping concentrations (from $1.0 \cdot 10^{14}$ to $1.0 \cdot 10^{16}$ cm⁻³) and at room temperature.

Observing the dependence of dark current density of the structure with the regrown InP NID doping level in Fig. 11, the leakage channel is clear since the higher the n doping on the regrown InP, the higher the current density at the interface, but the additional surface current does not have any contribution to the total dark current enough to justify the experimental observation, as can be seen in Fig. 10.

Thus, the calculation shows that the reduction of residual doping does result in reductions in the surface component of dark current, which is beneficial, although the residual doping should not be accounted as the main cause of the dark current being higher than expected. In this way, the cause of the surface current being higher than expected on the passivated deep mesas remains open.

5. Conclusions

In this work, the effect of different doping concentrations of the InP passivation layer on the dark current of a heterojunction photodiode was investigated. The results showed that a doping concentration in the range expected for residual doping for NID InP was not enough to increase the total dark current to the values measured. It shows that the residual doping is not the cause of the increase of dark current with the passivation even though the PL data shows a significant decrease in SRV, keeping the question open and requiring further investigation. It was also shown that decreasing the doping concentration of the regrown InP can help decrease the surface dark current, although it is not the main mechanism generating the dark current of the device and that the technique is still valid as a passivation method if the photodiode pixel is isolated by etching only the top contact layer.

Authors' statement

O.M.B: conceptualization, data curation, investigation, formal analysis, software, visualization, writing-review and editing, writing-original draft preparation. C.A.D.: data curation. R.M.S.K.: resources. L.D.P.: resources. G.S.V.: supervision, methodology, conceptualization, resources, writing-review and editing, validation, project administration, funding acquisition. M.P.P.: resources, project administration. P.L.S.: resources, project administration, funding acquisition, writing-review and editing. E.M.: data curation. J.A.C.: resources, writing-review and editing. S.K.: resources, writing-review and editing, project administration, funding acquisition.

Acknowledgements

The authors are thankful to the State University of Campinas (Unicamp) for providing all the necessary infrastructure support to conduct this simulation work with the Silvaco Atlas software and to the staff of the Nanotech West Laboratory of the OSU.

This study was financed in part by the FINEP (Funding Agency for Studies and Projects), the FAPESP (The São Paulo Research Foundation) – grant 2016/05516-3, the CAPES (Coordenação de Aperfeiçoamento de Pessoal de Nível Superior) – Finance Code 001, the FAPERJ (the Rio de Janeiro's Science Foundation), and the CNPq

(Brazilian National Council for Scientific and Technological Development).

References

- [1] Jones, H. G. *et al.* Thermal infrared imaging of crop canopies for the remote diagnosis and quantification of plant responses to water stress in the field. *Funct. Plant Biol.* **36**, 978 (2009). <https://doi.org/10.1071/FP09123>
- [2] Chan, V. W. S. Free-space optical communications. *J. Lightwave Technol.* **24**, 4750–4762 (2006). <https://opg.optica.org/jlt/abstract.cfm?URI=jlt-24-12-4750>
- [3] Green, R. O. *et al.* Imaging spectroscopy and the airborne visible/infrared imaging spectrometer (AVIRIS). *Remote Sens. Environ.* **65**, 227–248 (1998). [https://doi.org/10.1016/S0034-4257\(98\)00064-9](https://doi.org/10.1016/S0034-4257(98)00064-9)
- [4] Susa, N., Yamauchi, Y. & Kanbe, H. Punch-through type InGaAs photodiode fabricated by vapor-phase epitaxy. *IEEE J. Quantum Electron.* **16**, 542–545 (1980). <https://doi.org/10.1109/JQE.1980.1070525>
- [5] Pearsall, T. P. & Papuchon, M. The Ga_{0.47}In_{0.53}As homojunction photodiode – A new avalanche photodiode in the near infrared between 1.0 and 1.6 μm. *Appl. Phys. Lett.* **33**, 640–642 (1978). <https://doi.org/10.1063/1.90447>
- [6] Park, S. *et al.* Monolithic two-color short-wavelength InGaAs infrared photodetectors using InAsP metamorphic buffers. *Appl. Surf. Sci.* **581**, 152421 (2022). <https://doi.org/10.1016/j.apsusc.2022.152421>
- [7] Li, X. *et al.* High performance visible-SWIR flexible photodiode based on large-area InGaAs/InP PIN structure. *Sci. Rep.* **12**, 7681 (2022). <https://doi.org/10.1038/s41598-022-11946-7>
- [8] Huntington, A. S. Types of Avalanche Photodiode. in *InGaAs Avalanche Photodiodes for Ranging and Lidar* 1–92 (Elsevier, 2020). <https://doi.org/10.1016/B978-0-08-102725-7.00001-5>
- [9] Ettenberg, M. H. *et al.* Room temperature 640×512 pixel near-infrared InGaAs focal plane array. *Proc. SPIE* **4028**, 201–207 (2000). <https://doi.org/10.1117/12.391733>
- [10] Dolas, M. H., Atesal, O., Caliskan, M. D., Bek, A. & Ozbay, E. Low dark current diffusion limited planar type InGaAs photodetectors. *Proc. SPIE* **11129**, 111290D (2019). <https://doi.org/10.1117/12.2528666>
- [11] Ji, X. *et al.* Improvement of surface leakage current of 2.6 μm InGaAs photodetectors by using inductive coupled plasma chemical vapor deposition technology. *Jpn. J. Appl. Phys.* **54**, 04DG09 (2015). <https://doi.org/10.7567/JJAP.54.04DG09>
- [12] Zhou, Y. *et al.* Impact of SiN_x passivation on the surface properties of InGaAs photo-detectors. *J. Appl. Phys.* **118**, 034507 (2015). <https://doi.org/10.1063/1.4926736>
- [13] Braga, O. M. *et al.* Surface passivation of InGaAs/InP p-i-n photodiodes using epitaxial regrowth of InP. *IEEE Sensors J.* **20**, 9234–9244 (2020). <https://doi.org/10.1109/JSEN.2020.2987006>
- [14] Bishop, G. *et al.* nBn detectors based on InAs/GaSb type-II strain layer superlattice. *J. Vac. Sci. Technol. B* **26**, 1145 (2008). <https://doi.org/10.1116/1.2830627>
- [15] Braga, O. M. *et al.* Investigation of InGaAs/InP photodiode surface passivation using epitaxial regrowth of InP via photoluminescence and photocurrent. *Mater. Sci. Semicond. Process.* **154**, 107200 (2023). <https://doi.org/10.1016/j.mssp.2022.107200>
- [16] Chow, R. & Chai, Y. G. Electrical and optical properties of InP grown by molecular beam epitaxy using cracked phosphine. *Appl. Phys. Lett.* **42**, 383–385 (1983). <https://doi.org/10.1063/1.93947>
- [17] Glade, M., Hergeth, J., Grützmaier, D., Masseli, K. & Balk, P. Diffusion of Zn acceptors during MOVPE of InP. *J. Cryst. Growth* **108**, 449–454 (1991). [https://doi.org/10.1016/0022-0248\(91\)90221-P](https://doi.org/10.1016/0022-0248(91)90221-P)
- [18] SILVACO International. *ATLAS User's manual sees* (2018). http://ridl.cfd.rit.edu/products/manuals/Silvaco/atlas_users.pdf
- [19] Meiners, L. G. Electrical properties of SiO₂ and Si₃N₄ dielectric layers on InP. *J. Vac. Sci. Technol.* **19**, 373–379 (1981). <https://doi.org/10.1116/1.571066>
- [20] Levinshtein, M., Rumyantsev, S. & Shur, M. *Handbook Series on Semiconductor Parameters: Volume 2. Ternary and Quaternary III-V Compounds 2.* (WORLD SCIENTIFIC, 1996).
- [21] Forrest, S. R. & Kim, O. K. Deep levels in In_{0.53}Ga_{0.47}As/InP heterostructures. *J. Appl. Phys.* **53**, 5738–5745 (1982). <https://doi.org/10.1063/1.331462>

